RF ELECTRON GUNS WITH CONTROLLED LONGITUDINAL DISPERSION FOR ATTOSECOND UED

Y. Cheng*, Shanghai Institute of Applied Physics, Pudong, China
Ch. Feng, Q. Gu†, Shanghai Advanced Research Institute, Pudong, China

Abstract

We formulate the design of a UED-oriented RF gun as a constrained longitudinal-dynamics problem and obtain a nonuniform 2.33-cell S-band solution with controlled longitudinal dispersion. The representative solution, $(0.4, 0.93, 1)$, operated near 46 MV/m, brings the phases of maximum energy gain and minimum time of flight (TOF) into near coincidence and thereby yields a well-defined gun dispersion. Simulation tracking gives a gun-exit beam with 3.18 MeV kinetic energy, 80 fs rms bunch length, 0.1 pC charge, and normalized emittance of about 10 nm · rad. With a matched Double Bend Achromat (DBA) beamline used as the longitudinal transport, the bunch is compressed to 940 as rms with 10 fC charge at the sample. For RF-amplitude, RF-phase, charge, and magnet-field jitters of 0.05%, 0.2 ps, 3%, and 0.01% rms, respectively, the sample-plane arrival-time jitter is 600 as rms; source-only scans give 518 as rms from amplitude jitter and 167 as rms from phase jitter. These results show that the proposed model provides a direct route to RF guns specifically suited for attosecond UED.

INTRODUCTION

The temporal resolution of MeV ultrafast electron diffraction (UED) is limited jointly by the bunch duration and the shot-to-shot arrival-time jitter [1]. In present MeV UED beamlines, the RF gun remains one of the dominant sources of timing noise. The widely used 1.6-cell photoinjector was originally developed for FEL injectors and is highly effective for producing low projected energy spread, but its exit momentum and time of flight are not cleanly correlated [2]. As a result, RF phase and amplitude fluctuations are readily transferred into timing jitter. Downstream isochronous transport can compensate part of the momentum-dependent timing variation [3, 4], but a design principle for an RF gun specifically aimed at UED has remained lacking.

This work addresses that gap. We formulate the design of a UED-oriented RF gun as a constrained longitudinal-dynamics problem. The target is not minimum energy spread alone; rather, the gun is required to operate near a phase at which maximum energy gain and minimum TOF nearly coincide, so that the gun exit acquires a clean momentum–TOF correlation and admits a characteristic dispersion R_{56}^{g}. The model naturally yields a nonuniform 2.33-cell solution. We then analyze its longitudinal response, compare it directly with the conventional 1.6-cell gun, and verify with a DBA beamline that the resulting source supports attosecond-level compression and sub-femtosecond timing stability at the sample.

THEORETICAL MODEL

We formulate the RF-gun design as a constrained longitudinal-dynamics problem. For an N-cell gun, the cell lengths are written as

$$L_i = \alpha_i \frac{\lambda}{2}, \qquad L(\alpha) = \sum_{i=1}^{N} L_i, \tag{1}$$

where α_i is the dimensionless cell-length parameter and $\lambda = c/f$ is the RF wavelength. Let E_0 denote the peak accelerating field and ϕ_0 the launch phase at the cathode. With $\psi(z) = \omega t - kz + \phi_0$, where $k = \omega/c = 2\pi/\lambda$ is the RF wave number, the longitudinal dynamics is governed by

$$\begin{aligned} &\frac{d\gamma}{dz} = \frac{eE_0}{mc^2} u(z;\alpha)\sin\psi, \qquad \frac{d\psi}{dz} = k\left(\frac{1}{\beta} - 1\right), \\ &\frac{dt}{dz} = \frac{1}{c\beta}, \end{aligned} \tag{2}$$

which define the exit kinetic energy $W(\alpha, E_0, \phi_0) = mc^2[\gamma(L) - 1]$ and the time of flight $T(\alpha, E_0, \phi_0) = t(L)$. The design condition is imposed at a common operating phase ϕ^* by

$$\begin{aligned} W(\alpha, E_0, \phi^*) &= W^*, \\ \partial_\phi W(\alpha, E_0, \phi^*) &= 0, \\ \partial_\phi T(\alpha, E_0, \phi^*) &= 0. \end{aligned} \tag{3}$$

For the present design we consider a three-cell structure, $\alpha = (\alpha_1, \alpha_2, \alpha_3)$. Three cells are sufficient to separate the three physical roles required here: the first cell controls the early nonrelativistic phase slippage, the second cell adjusts the transition into the high-energy regime, and the third cell provides the final near-relativistic energy gain. The first cell is shortened because the beam is still far from relativistic immediately after emission, so the phase advance accumulated there has the largest leverage on the relative location of the maximum-energy and minimum-TOF phases. The second cell is retained close to a full cell and only weakly tuned, because its role is to compensate the phase-slip change introduced by the shortened first cell while preserving efficient acceleration and field balance. The third cell is fixed as a standard full cell, $\alpha_3 = 1$, since by that stage the beam is already near relativistic and the cell contributes mainly stable energy gain, with little further leverage on phase alignment.

With α_3 fixed, the problem remains underdetermined because the unknowns still include $(\alpha_1, \alpha_2, E_0, \phi^*)$. We therefore introduce the closure functional

$$J(\alpha_1, \alpha_2, E_0) = E_0^2 + \mu(\alpha_2 - 1)^2, \qquad \mu > 0, \tag{4}$$

* also at University of Chinese Academy of Sciences, Beijing, China
† guq@sari.ac.cn

which favors lower operating field and a second cell remaining close to a standard full cell. The target energy $W^* = 3.18\,\mathrm{MeV}$ is chosen as the operating energy at which the fixed DBA layout, including finite-energy drift dispersion and the gun-defined R_{56}^{g}, satisfies first-order cathode-to-sample isochronicity. It remains close to the 3 MeV DBA working point of Ref. [7], while avoiding the over- or under-compensation produced when the drift contribution changes with beam energy. The representative solution is $(\alpha_1, \alpha_2, \alpha_3) \approx (0.4, 0.93, 1)$ with $E_0 \approx 46\,\mathrm{MV/m}$, and the operating phase is located near 65°. Thus E_0 is not an independently selected field value; it is the field required to reach W^* while simultaneously satisfying the two phase-stationarity constraints and keeping α_2 close to a full cell.

Following the one-dimensional approximate treatment of Kim [5], we further retain the reduced phase-slippage description associated with the shortened first cell. Defining

$$u_1(\phi_0) = \frac{eE_0L_1}{mc^2}\sin\phi_0, \qquad t_1 = \frac{L_1}{u_1 c}\sqrt{u_1(2+u_1)}, \quad (5)$$

and

$$\Psi_1(\phi_0) = kL_1\frac{\sqrt{u_1(2+u_1)}}{u_1}, \quad (6)$$

where Ψ_1 denotes the phase advance accumulated across the shortened first cell, the high-energy operating phase is obtained from

$$\left(\Psi_1 - \phi_a^*\right)\sin\phi_a^* \simeq \frac{mc^2k}{eE_0}. \quad (7)$$

For $f = 2.856\,\mathrm{GHz}$, $E_0 \approx 46\,\mathrm{MV/m}$, and $(\alpha_1, \alpha_2, \alpha_3) \approx (0.4, 0.93, 1)$, Eq. (7) yields the high-energy branch $\phi_a^* \approx 64°$, consistent with the operating phase obtained from the global constrained formulation.

At the same level of approximation, the whole-gun energy is estimated by

$$K_a \simeq \eta_{\mathrm{gun}}\, eE_0L_{\mathrm{tot}}\sin\phi_a^*, \qquad L_{\mathrm{tot}} = L_1 + L_2 + L_3, \quad (8)$$

where η_{gun} is the transit-time/envelope factor of the standing-wave field, not a fitted normalization. In a simplified TM_{010}-envelope model, a synchronous particle samples the axial field as $|\cos(\pi z/L_{\mathrm{tot}})|$ rather than as a flat field, giving $\eta_{\mathrm{gun}} \simeq 2/\pi$. Thus $K_a \simeq (2/\pi)eE_0L_{\mathrm{tot}}\sin\phi_a^*$. Substituting $E_0 \approx 46\,\mathrm{MV/m}$, $L_{\mathrm{tot}} \approx 0.1223\,\mathrm{m}$, and $\phi_a^* \approx 64°$ gives $K_a \approx 3.2\,\mathrm{MeV}$, in agreement with the constrained target $W^* = 3.18\,\mathrm{MeV}$.

LONGITUDINAL DISPERSION OF THE 2.33-CELL RF GUN

The representative solution obtained from Sec. II is a nonuniform 2.33-cell S-band RF gun with $(\alpha_1, \alpha_2, \alpha_3) \approx (0.4, 0.93, 1)$, operated near $E_0 \approx 46\,\mathrm{MV/m}$. All particle-tracking simulations in this work were performed with the General Particle Tracer (GPT) [6] code. The defining longitudinal property of this gun is the near coincidence of the phases for maximum energy gain and minimum time of flight (TOF).

Figure 1 shows the on-axis field profile together with the phase dependence of the gun-exit beam properties. The shortened first cell shifts the phase slippage while the beam is still nonrelativistic, where the TOF is most sensitive to the launch phase. The second cell compensates the resulting phase displacement and restores efficient acceleration without undoing the phase alignment established upstream. The third cell mainly provides stable final energy gain. As a result, the phase of maximum gun-exit energy is driven toward the phase of minimum TOF. For the present gun, both occur in the high-phase region around 63° to 65°, where the beam exits the gun at about 3.18 MeV. This near coincidence is the central longitudinal feature of the 2.33-cell gun.

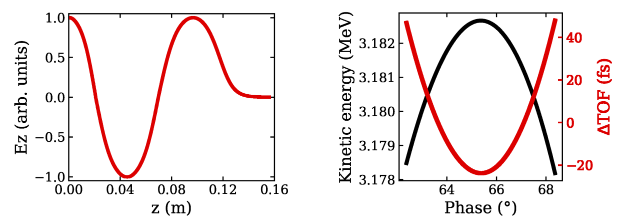

(a) (b)

Figure 1: Longitudinal response of the nonuniform 2.33-cell RF gun: (a) on-axis accelerating field; (b) phase dependence of gun-exit energy and TOF. The maximum-energy and minimum-TOF phases fall in the same high-phase region near 3.18 MeV.

Figure 2 compares the gun-exit timing response of a conventional 1.6-cell gun and the present 2.33-cell gun under RF phase jitter of ± 0.2 ps and RF-amplitude jitter of $\pm 10^{-3}$. In the 1.6-cell gun, the phase of maximum energy and that of minimum TOF are separated, so the gun-exit TOF and momentum do not form a unique correlation. The blue circles represent amplitude perturbations at fixed RF phase, and the red squares represent phase perturbations at fixed RF amplitude. Under simultaneous amplitude and phase perturbations, the cloud therefore spreads in two partially independent directions, showing that the 1.6-cell gun does not admit a cleanly defined gun dispersion.

In the 2.33-cell gun, by contrast, the near overlap of the maximum-energy and minimum-TOF phases collapses the gun-exit response onto an almost one-to-one energy–TOF curve. Both amplitude and phase perturbations are funneled onto the same longitudinal correlation, so the gun can be characterized by an effective longitudinal dispersion,

$$\Delta t_g \simeq \frac{R_{56}^{g}}{c}\,\delta, \qquad \delta = \frac{\Delta p}{p}, \quad (9)$$

with $R_{56}^{g} \approx -2.1\,\mathrm{cm}$. In this regime the first-order sensitivity to RF phase fluctuations is strongly reduced, whereas the residual timing variation remains predominantly amplitude driven and directly correlated with beam momentum.

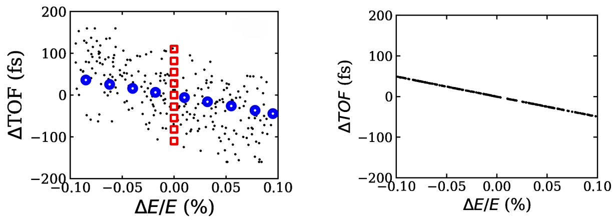

(a) (b)

Figure 2: Gun-exit TOF as a function of relative energy deviation under RF phase jitter of ±0.2 ps and RF-amplitude jitter of $\pm 10^{-3}$. In the 1.6-cell gun, the emphasized blue circles denote amplitude perturbations at fixed phase and the red squares denote phase perturbations at fixed amplitude; the two sets do not collapse onto a unique curve. In the 2.33-cell gun, the response is compressed onto an almost one-to-one curve, allowing the definition of R_{56}^{g}.

SIMULATION RESULTS

Following the DBA concept of Ref. [7], the downstream transport is matched to the gun-defined longitudinal state through

$$R_{56}^{\mathrm{tot}} = R_{56}^{\mathrm{gun}} + R_{56}^{\mathrm{u}} + R_{56}^{\mathrm{DBA}} + R_{56}^{\mathrm{d}}. \tag{10}$$

When $R_{56}^{\mathrm{tot}} \approx 0$, the momentum-dependent timing modulation generated at the gun exit is compensated by the downstream transport. This condition is meaningful only because the 2.33-cell gun provides a clean momentum–TOF correlation and therefore a well-defined R_{56}^{gun}.

Figure 3 shows the cathode-to-sample timing response of the 2.33-cell gun matched to the DBA transport. Panel (a) gives the beam energy as a function of RF amplitude and phase, while panel (b) gives the relative cathode-to-sample TOF. Panels (c) and (d) are the derivatives of the TOF in panel (b) with respect to RF amplitude and RF phase, respectively. The highlighted dashed guide lines mark the operating conditions under which the sample arrival time is insensitive to RF-amplitude or RF-phase fluctuations. The operating point is given by the intersection of the dashed lines, where the cathode-to-sample TOF is synchronized and the corresponding RF amplitude and phase define the nominal gun setting.

For the GPT tracking reported here, the cathode laser distribution used an rms transverse spot size of 100 µm and an rms pulse length of 50 fs; the gun-exit beam has a kinetic energy of 3.18 MeV, an rms bunch length of 80 fs, a charge of 0.1 pC, and a normalized emittance of about 10 nm · rad. The single-particle timing maps used to determine R_{56}^{g} and the cathode-to-sample sensitivities were calculated without space charge. The full-bunch GPT tracking used for compression includes the space-charge force, which generates the correlated energy chirp and also contributes to the residual compression-stage evolution. The matched transport uses a 1.8 m drift from the gun exit to the DBA entrance and a 0.78 m drift from the DBA exit to the sample; including the DBA, the sample is located about 3.3 m downstream of the gun exit. Transverse focusing in the downstream beamline is provided by the gun solenoid and the DBA quadrupoles.

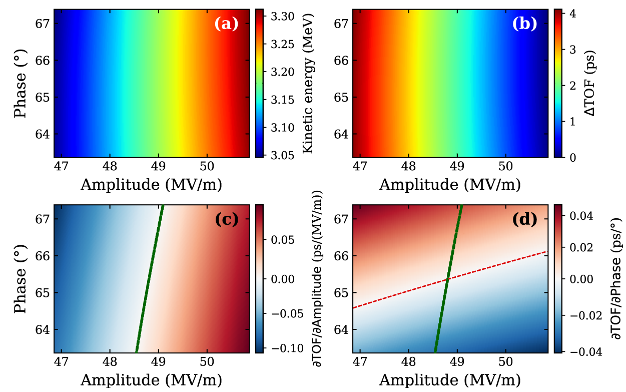

Figure 3: Cathode-to-sample timing response of the 2.33-cell gun matched to the DBA transport: (a) beam energy; (b) relative cathode-to-sample TOF; (c) derivative of TOF with respect to RF amplitude; (d) derivative of TOF with respect to RF phase. The dashed curves mark the zero-sensitivity conditions used to locate the synchronized operating point.

No additional longitudinal phase-space manipulation element is included in the present simulation; the compression and timing stabilization are produced by the gun-induced energy–time correlation and the matched DBA longitudinal transport.

Using the DBA transport parameters following Ref. [7], the beam is compressed to 940 as rms at the sample with a remaining charge of about 10 fC. Under RF-amplitude, RF-phase, charge, and magnet-field jitters of 0.05%, 0.2 ps, 3%, and 0.01% rms, respectively, the sample-plane arrival-time jitter is 600 as rms. When the source jitters are scanned independently, the timing jitter is 518 as rms from RF-amplitude jitter alone and 167 as rms from RF-phase jitter alone. The amplitude-driven term therefore remains dominant, while the phase-driven term is strongly reduced by the near coincidence of the maximum-energy and minimum-TOF phases. Under the same matched condition, the bunch is simultaneously compressed into the attosecond regime, indicating that the 2.33-cell gun possesses the longitudinal response required for attosecond UED.

CONCLUSION

We have presented a constrained design model for RF guns with controlled longitudinal dispersion and shown that it naturally yields a UED-oriented nonuniform 2.33-cell solution. The three-cell structure separates the roles of low-energy phase slippage, transition matching, and stable final acceleration, while the shortened first cell brings the phases of maximum energy gain and minimum TOF into near coincidence. The resulting gun exhibits a clean gun-exit energy–TOF correlation and a characteristic dispersion R_{56}^{g}. GPT tracking with a matched DBA beamline gives a compressed bunch length of 940 as rms and a sample-plane arrival-time jitter of 600 as rms. These results show that controlled gun longitudinal dispersion provides a direct route to attosecond MeV-UED.

REFERENCES

[1] R. Srinivasan, V. A. Lobastov, C.-Y. Ruan, and A. H. Zewail, "Ultrafast electron diffraction (UED): A new development for the 4D determination of transient molecular structures," *Helv. Chim. Acta*, vol. 86, no. 6, pp. 1761–1799, 2003. doi:10.1002/hlca.200390147

[2] J. B. Hastings et al., "Ultrafast time-resolved electron diffraction with megavolt electron beams," *Appl. Phys. Lett.*, vol. 89, no. 18, p. 184109, 2006. doi:10.1063/1.2372697

[3] Y. Cheng, Q. Gu, and C. Feng, "Multidimensional phase space manipulation for attosecond electron bunch compression," *Phys. Rev. Accel. Beams*, 2026. doi:10.1103/3t5l-mz61

[4] H. W. Kim et al., "Towards jitter-free ultrafast electron diffraction technology," *Nat. Photonics*, vol. 14, no. 4, pp. 245–249, 2020. doi:10.1038/s41566-019-0566-4

[5] K.-J. Kim, "RF and space-charge effects in laser-driven rf electron guns," *Nucl. Instrum. Methods Phys. Res. A*, vol. 275, no. 2, pp. 201–218, 1989. doi:10.1016/0168-9002(89)90688-8

[6] S. B. van der Geer and M. J. de Loos, "The general particle tracer code: Design, implementation and application," Ph.D. thesis, Technische Universiteit Eindhoven, 2001. doi:10.6100/IR542912

[7] F. Qi et al., "Breaking 50 femtosecond resolution barrier in MeV ultrafast electron diffraction with a double bend achromat compressor," *Phys. Rev. Lett.*, vol. 124, no. 13, p. 134803, 2020. doi:10.1103/PhysRevLett.124.134803